Computers and Geotechnics 40 (2012) 89–96

Contents lists available at SciVerse ScienceDirect

Computers and Geotechnics

journal homepage: www.elsevier.com/locate/compgeo

Technical Communication

Predicting effective stress parameter of unsaturated soils using neural networks

Mohsen Ajdari [1], Ghassem Habibagahi *, Arsalan Ghahramani [2]

Department of Civil Eng., School of Eng., Shiraz University, Zand Street, Shiraz 7134851156, Iran

ARTICLE INFO

Article history:
Received 24 April 2011
Received in revised form 12 September 2011
Accepted 22 September 2011
Available online 10 November 2011

Keywords:
Unsaturated soil
Neural networks
Effective stress parameter

ABSTRACT

In the effective stress equation for unsaturated soils proposed by Bishop, shear strength in these soils depends on the effective stress parameter, χ, a function of soil suction [1]. To estimate the shear strength of unsaturated soils, one must already know this parameter and its variation with soil suction. Though theories on the shear strength of unsaturated soils are consistent with experimental measurements, estimating the effective stress parameter directly from tedious laboratory tests is impractical. Thus, researchers have performed numerous intensive studies to effectively obtain the unsaturated shear strength using simplified empirical methods.

This paper shows an adaptive learning neural network method for predicting this parameter, χ. The proposed network is a multilayer perceptron network with six neurons in the input layer representing the air entry value, the volumetric water content at residual and saturated conditions, the slope of soil water characteristic curve, the net confining stress and suction. The available literature uses a database prepared from triaxial shear test results to train and test the network. The results show the suitability of the proposed approach for estimating the effective stress parameter. Network analysis indicates that the χ-parameter depends strongly on the net mean stress.

1. Introduction

Evaluation of the soil shear strength is an important step in the stability analysis of earth structures, foundations and natural slopes; a cost-optimized design requires accurate shear strength prediction in unsaturated soils. Assuming Mohr–Coulomb failure criteria, the shear strength of soils is:

$$\tau = \sigma' \tan(\phi') + c' \tag{1}$$

where τ is the shear strength, σ' is the effective normal stress on failure plane and c' and ϕ' are the effective shear strength parameters of the soil. Effective stress for unsaturated soils is written as follows [1]:

$$\sigma' = (\sigma - u_a) + \chi(u_a - u_w) \tag{2}$$

where σ is total stress, u_a is pore air pressure, u_w is pore water pressure and χ is an effective stress parameter: 0 for completely dry soils and 1 for fully saturated soils.

The effective stress parameter and resulting shear strength of unsaturated soils depend on soil properties. Some researchers claim that the assumption $\chi = S_r$ can predict the shear strength of unsaturated soils [2] but the effective stress parameter and shear strength of unsaturated soils depend on soil structure and properties [3]. Properties of unsaturated soils can be simply determined using the soil water characteristic curve (SWCC). Several empirical approaches have thus been introduced recently to predict the shear strength of unsaturated soils with the SWCC. Fredlund et al. proposed the following relationship to predict the shear strength of unsaturated soils based on two independent stress state variables [4]:

$$\tau = c' + (\sigma - u_a)\tan\phi' + (u_a - u_w)\tan\phi'\left(\frac{\theta - \theta_r}{\theta_s - \theta_r}\right) \tag{3}$$

where θ is the volumetric water content at critical state, θ_r is the residual volumetric water content and θ_s is the volumetric water content at saturated condition. Vanapalli et al. proposed a similar equation [5]:

$$\tau = c' + (\sigma - u_a)\tan\phi' + (u_a - u_w)\tan\phi'(\bar{\theta})^{\kappa} \tag{4}$$

where κ is a fitting parameter and $\bar{\theta}$ equals $\frac{\theta}{\theta_s}$. Garven and Vanapalli found a relationship between κ and the plasticity index of the soil [6]. The test results demonstrated both that the net confining pressure significantly influences the SWCC and parameters of this curve vary with stress changes [7]. Therefore, the net stress effect on the saturated and residual water content should be taken into account in Eqs. (3) and (4).

Khalili and Khabbaz demonstrated that the effective stress parameter (χ) is unity at suctions below bubbling pressure and

* Corresponding author. Tel.: +98 9173138193; fax: +98 7116286619.
E-mail addresses: ajdari@shirazu.ac.ir (M. Ajdari), habibg@shirazu.ac.ir (G. Habibagahi), ghahrama@shirazu.ac.ir (A. Ghahramani).
[1] Tel.: +98 9173196516; fax: +98 7116286619.
[2] Tel.: +98 9171170101; fax: +98 7116286619.

0266-352X/$ - see front matter © 2011 Elsevier Ltd. All rights reserved.
doi:10.1016/j.compgeo.2011.09.004

that the relationship between χ and the matric suction logarithm is linear [8]. Based on these observations, they proposed a new equation for χ:

$$\chi = \left(\frac{(u_a - u_w)}{(u_a - u_w)_b}\right)^{\gamma} \tag{5}$$

where $(u_a - u_w)_b$ is the air entry value in the drying process and equals the air expulsion value in the wetting condition. Parameter γ varies from -0.4 (lower bound of the equation) to -0.65 (upper bound), averaging -0.55. Xu found a similar formula for the effective stress parameter using fractal theory [9]. Here, the SWCC could estimate the soil's surface fractal dimension.

Russell and Khalili developed the following equation for sand [10]:

$$\chi = \begin{cases} 1 & \text{for } \frac{(u_a-u_w)}{(u_a-u_w)_b} < 1 \\ \left(\frac{(u_a-u_w)}{(u_a-u_w)_b}\right)^{-0.55} & \text{for } 1 < \frac{(u_a-u_w)}{(u_a-u_w)_b} < 25 \\ 25^{0.45}\left(\frac{(u_a-u_w)}{(u_a-u_w)_b}\right)^{-1} & \text{for } \frac{(u_a-u_w)}{(u_a-u_w)_b} > 25 \end{cases} \tag{6}$$

Zargarbashi and Khalili demonstrated that the stress state influences the bubbling pressure and this parameter's corrected value should be utilized to precisely estimate the χ-parameter [11]. Additionally, evaluating the various empirical relationships has shown that none can successfully predict the shear strength of all types of unsaturated soils [6,12].

Arvin et al. developed a numerical method based on the percolation theory to estimate the effective stress parameter [13]. Here, the SWCC determined the pore size distribution in the soil and the authors constructed a conceptual model from the percolation theory. The conceptual model directly determines the effective stress parameter, but this method needs high-performance computer systems to extend the prediction domain to a high suction range.

Recently, some researchers used the Artificial Neural Network (ANN) to relate the shear strength of unsaturated soils and their physical properties [14,15]. However, their model does not account for the influence of the sample preparation method and its stress state. Processing the triaxial unsaturated shear test results shows that the effective stress parameter changes significantly when net mean stress changes and suction remain constant. Fig. 1 shows the effect of net mean stress on the effective stress parameter of Kurnell sand [10,16].

The ANN can consider several input parameters and find a nonlinear estimation with them. The authors selected this technique to estimate the effective stress parameter (χ) required to properly estimate the shear strength of unsaturated soils. The network input variables include the matric suction, net mean stress and SWCC parameters of the soil. The following section explains these parameters. This paper also analyzes the effect of net stress on the effective stress parameter.

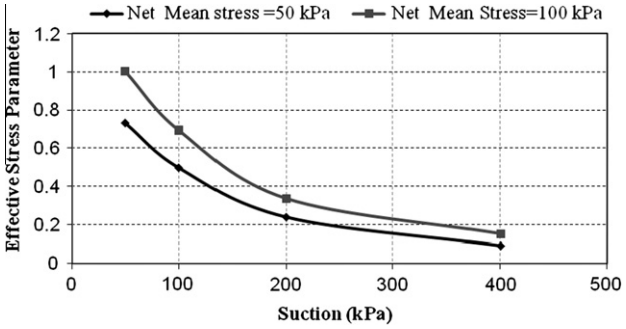

Fig. 1. Effect of net mean stress on the effective stress parameter of the Kurnell Sand (raw data from Russell and Khalili [16,10]).

2. Soil water characteristic curve

Matric suction is important when calculating shear strength. This parameter is usually determined by the difference between pore air and pore water pressures. The relationship between water content and matric suction is the SWCC. The SWCC represents the soil structure, and is therefore usually a tool to estimate the permeability and shear strength of unsaturated soils (Eqs. (3)–(6)).

The SWCC defines several parameters: saturated volumetric water content, θ_s, bubbling pressure, $(u_a - u_w)_b$, and residual water content, θ_r [17]. Based the soil water characteristic curve, one can identify three different stages in the soil desaturation process [18].

In the first stage, the suction value is less than the bubbling pressure and the soil media is still saturated. The soil's shear strength increases linearly with suction in this stage. The effective stress parameter equals one and Terzaghi's effective stress describes the soil's mechanical behavior [19].

After exceeding the suction point where air first enters the largest exposed soil pores (air entry value), the soil's water content decreases significantly and the second portion of the SWCC commences. There is a nonlinear increase in shear strength for the range of suction values associated with the second part of SWCC.

The third part of the SWCC commences with residual water content. In comparison with the second part of SWCC, a large increase in suction leads to a relatively small change in moisture content. The experimental investigations show that shear strength can increase, decrease or remain constant beyond the residual water content [20].

Researchers have suggested various empirical equations to describe the SWCC. Among them, the relationships proposed by Brooks and Corey [21], van Genuchten [22] and Fredlund and Xing [23] have been used widely in geotechnical engineering. The Brooks and Corey simulation, adopted in this study, is simpler through physically meaningful parameters [21]:

$$\begin{cases} \frac{\theta-\theta_r}{\theta_s-\theta_r} = \left(\frac{(u_a-u_w)_b}{u_a-u_w}\right)^{\lambda} & \text{for } (u_a - u_w) \geqslant (u_a - u_w)_b \\ \theta = \theta_s & \text{for } (u_a - u_w) \leqslant (u_a - u_w)_b \end{cases} \tag{7}$$

Here, λ is a fitting parameter, and θ_s and θ_r are as defined before. To comprehensively describe the soils' SWCCs, all parameters (θ_s, θ_r, $(u_a - u_w)_b$ and λ) were determined and introduced to the neural network, as explained in the next section.

3. Neural network method

A multi-layer perceptron network generally consists of parallel layers of artificial units (neurons) associated by connections (Fig. 2): a set of input neurons, one or more hidden layers and the output layer. Each connection transmits a signal to a neuron in the next layer through a feed-forward algorithm. Each signal is multiplied by the connection weight and a sigmoid activation function is applied to the sum of the weighted signals and the bias through this transition process. The number of neurons in each layer controls the subscript of the weight matrices. Eq. (8) shows the calculation procedure performed by a typical neural network to find the output vector:

$$h_{1,m} = f\left(\sum_{p=1}^{n}(i_{1,p}w_{p,m}) + b_m\right) \tag{8-a}$$

$$o_{1,m} = f'\left(\sum_{q=1}^{m}(h_{1,q}w'_{p,m}) + b_r\right) \tag{8-b}$$

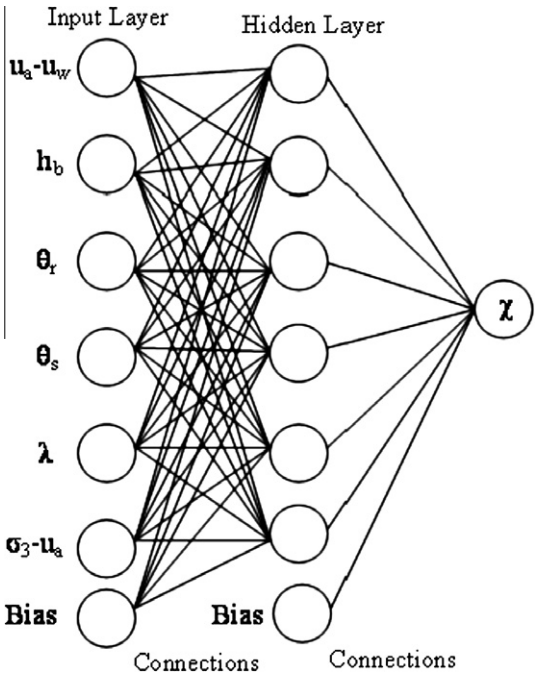

Fig. 2. Schematic layout of the ANN model 1.

Here, i, h and o represent the value of the input, hidden and output neurons, respectively; f and f' are activation functions and n, m and r are the number of input, hidden and output neurons, correspondingly. w and w' symbols represent the weight matrices and b is the weighted bias. The output layer presents the solution to the problem.

The first stage of the neural network methodology is performing calculations on known input signals to determine the network's connection weights to determine the closest final output to the known target value [24]. These calculations are the training stage. The network's designer usually selects the activation functions and the learning stage generally determines the weights and biases assigned to the network's connections. The most common learning method is the back propagation algorithm. In this method, the weights and biases update in the direction of the negative gradient of the average error between the network output and the target output:

$$w_{k+1} = w_k - \alpha_k e_k \tag{9}$$

Here, w_k is a vector of current weights and biases, e_k is the current gradient and α_k is the rate of learning. The network's weights and biases only update after the entire training set is presented to the network (batch mode approach).

The basic methodology of the artificial neural network generally includes a network testing stage with the training process. A new data set, unexposed to the network during the training stage, is presented to the trained network and the outputs are compared with the target values. The average error indicates the trained network's performance. The trained network can simply predict the output (solution to the problem) for a new set of input data using Eqs. (8-a) and (8-b).

This study used a three-layer feed-forward back propagation neural network. The initial weights and biases connecting neurons of the input layer, hidden layer and output layer are usually assigned randomly. To provide an intelligent weight initialization, this investigation used the Nguyen–Widrow method [25]. The network was trained by a training function that updates weight and bias values according to the Levenberg–Marquardt adaptive optimization method [26,27]. Input and output data sets were normalized using the min–max approach. The MATLAB computer-aided software toolbox (2004) was employed for the neural network process [28].

The input layer consisted of six neurons, representing the bubbling pressure, the volumetric water content at both residual and saturated conditions, the λ parameter, the net confining stress, and suction. The bubbling pressure and water content at saturation conditions were determined directly from the SWCCs, while the other two parameters, λ and θ_r, were determined by fitting Eq. (7) to the data points.

Data from the literature's triaxial shear and pressure plate/filter paper test results were used to train and test the network. The results from 100 consolidated drained (CD) triaxial shear tests performed on 14 different soil types were collected from the literature and employed to train the network to determine the effective stress parameter under different suctions. Table 1 indicates the properties of the soils employed in this study.

The network was further tested using another database containing 21 constant water (CW) data sets obtained from triaxial shear tests on different soil (Table 2). Due to hydraulic hysteresis, the SWCC has two different branches: one corresponds to adsorption and the other to desorption. The soil tends to dilate and absorb water during the softening phenomenon. However, the soil behavior in the strain hardening condition is characterized by a reduction in volume accompanied by flow of water out of the soil specimen. Hence, the drying branch of the SWCC should be employed for CW tests in the strain hardening condition, and the wetting branch of the SWCC should be used if the strain softening and strength drop occur.

4. Results and discussion

The ANN was trained using the results from 100 constant suction CD triaxial shear tests and tested using 21 CW tests' results, unexposed to the network during the training phase. The optimal number of hidden layers and neurons was determined in a trial by increasing the number of neurons and monitoring the network performance. It was unnecessary to stop the procedure early and the number of epochs was limited to 500, as there was no considerable reduction in the error measure below this point.

Figs. 3 and 4 compare the predicted values of the effective stress parameter with the actual values for the training and testing data, respectively. These figures demonstrate good agreement between the predictions made by ANN modeling and the actual values for the effective stress parameter for both training and testing data. Based on these results, the NN model produces reasonable predictions for CW tests that experienced a different stress path and were not exposed to the network during the training procedure.

The values of axial stress at failure determined using the predicted effective stress parameters for the above data set were compared with the actual shear strengths. The results are in Figs. 5 and 6:

$$\sigma'_1 = \sigma'_3 \tan^2\left(45 + \frac{\phi'}{2}\right) + 2c' \tan\left(45 + \frac{\phi'}{2}\right) \tag{10}$$

Here, σ'_1 and σ'_3 are axial and confining stresses at failure condition, respectively. Table 3 shows the shear strength parameters (c' and ϕ') of the studied soils. These figures indicate good agreement between the model's prediction and the actual shear strength for both training and testing data. Because Bishop and Blight exclusively presented χ values without the shear test results [30], their shear strengths are absent in Fig. 5.

To assess the importance of input parameters on the network's performance, each parameter was eliminated from the input layer

Table 1
Soil properties of data base for training ANN.

Reference	Net confining pressure (kPa)	Suction (kPa)	χ	h_b (kPa)	θ_r	θ_s	λ
[29]	50	50	1	100	0.171	33.1	0.89
[29]	100	50	1	100	0.171	33.1	0.89
[29]	150	50	1	100	0.171	33.1	0.89
[29]	50	100	1	100	0.171	33.1	0.89
[29]	100	100	1	100	0.171	33.1	0.89
[29]	150	100	1	100	0.171	33.1	0.89
[29]	50	150	0.7024	100	0.171	33.1	0.89
[29]	100	150	0.6737	100	0.171	33.1	0.89
[29]	150	150	0.8582	100	0.171	33.1	0.89
[7]	0	0	1	2.5	8.065	36	0.62
[7]	150	0	1	2.5	8.065	36	0.62
[7]	300	0	1	2.5	8.065	36	0.62
[7]	0	50	0.3562	2.5	8.065	36	0.62
[7]	150	50	0.3733	2.5	8.065	36	0.62
[7]	300	50	0.3678	2.5	8.065	36	0.62
[7]	0	100	0.2348	2.5	8.065	36	0.62
[7]	150	100	0.3228	2.5	8.065	36	0.62
[7]	300	100	0.3541	2.5	8.065	36	0.62
[7]	0	200	0.1741	2.5	8.065	36	0.62
[7]	150	200	0.2465	2.5	8.065	36	0.62
[7]	300	200	0.2905	2.5	8.065	36	0.62
[7]	0	300	0.1463	2.5	8.065	36	0.62
[7]	150	300	0.1832	2.5	8.065	36	0.62
[7]	300	300	0.2504	2.5	8.065	36	0.62
[30]	0	377.4	0.11	7.4	0	23.82	0.19
[30]	0	95.2	0.41	7.4	0	23.82	0.19
[30]	0	57.8	0.6	7.4	0	23.82	0.19
[30]	0	30.6	0.74	7.4	0	23.82	0.19
[30]	0	180.2	0.27	7.4	0	23.82	0.19
[30]	0	16.32	0.9	7.4	0	23.82	0.19
[30]	0	20.4	0.79	7.4	0	23.82	0.19
[30]	204	612	0.24	7.4	0	23.82	0.19
[30]	204	527	0.26	7.4	0	23.82	0.19
[30]	204	496.4	0.35	7.4	0	23.82	0.19
[30]	204	455.6	0.32	7.4	0	23.82	0.19
[30]	204	442	0.49	7.4	0	23.82	0.19
[30]	204	214.2	0.53	7.4	0	23.82	0.19
[30]	204	44.2	0.9	7.4	0	23.82	0.19
[30]	0	47.6	0.47	44.7	21.54	34.76	0.96
[30]	0	27.2	1	44.7	21.54	34.76	0.96
[30]	0	34	1	44.7	21.54	34.76	0.96
[30]	0	17	1	44.7	21.54	34.76	0.96
[30]	0	20.4	1	44.7	21.54	34.76	0.96
[30]	0	13.6	1	44.7	21.54	34.76	0.96
[30]	0	12.58	1	44.7	21.54	34.76	0.96
[30]	0	13.6	1	44.7	21.54	34.76	0.96
[30]	0	30.6	1	44.7	21.54	34.76	0.96
[31]	200	100	0.6462	95	23.67	34.58	0.48
[31]	200	200	0.5755	95	23.67	34.58	0.48
[31]	200	100	1	125	28.35	39.72	0.91
[31]	200	200	0.6883	125	28.35	39.72	0.91
[31]	200	400	0.57	125	28.35	39.72	0.91
[31]	200	100	1	200	20.58	32.47	1.05
[31]	200	200	1	200	20.58	32.47	1.05
[31]	200	400	0.7283	200	20.58	32.47	1.05
[32]	30	20	0.8938	2.5	5.206	38	1.11
[32]	30	60	0.4966	2.5	5.206	38	1.11
[32]	30	100	0.3575	2.5	5.206	38	1.11
[32]	125	20	0.8938	2.5	5.206	38	1.11
[32]	125	60	0.6952	2.5	5.206	38	1.11
[32]	125	100	0.5363	2.5	5.206	38	1.11
[32]	250	20	1	2.5	5.206	38	1.11
[32]	250	60	0.9931	2.5	5.206	38	1.11
[32]	250	100	0.5959	2.5	5.206	38	1.11
[32]	30	20	0.7151	7	0	38	0.41
[32]	30	60	0.4966	7	0	38	0.41
[32]	30	100	0.4052	7	0	38	0.41
[32]	125	60	0.8541	7	0	38	0.41
[32]	125	20	1	7	0	38	0.41
[32]	125	100	0.7151	7	0	38	0.41
[32]	250	20	0.8938	7	0	38	0.41
[32]	250	60	0.8938	7	0	38	0.41
[32]	250	100	0.7151	7	0	38	0.41
[33]	0	300	0.4801	47	3.462	52	0.73

Table 1 (*continued*)

Reference	Net confining pressure (kPa)	Suction (kPa)	χ	h_b (kPa)	θ_r	θ_s	λ
[33]	0	200	0.6481	47	3.462	52	0.73
[33]	0	100	0.9762	47	3.462	52	0.73
[34]	20	80	0.5795	30	28.31	55.95	0.33
[34]	70	80	0.7671	30	28.31	55.95	0.33
[34]	120	80	1	30	28.31	55.95	0.33
[34]	30	50	0.8717	30	28.31	55.95	0.33
[34]	50	50	1	30	28.31	55.95	0.33
[34]	100	50	1	30	28.31	55.95	0.33
[34]	80	120	0.8494	30	28.31	55.95	0.33
[34]	130	120	0.7938	30	28.31	55.95	0.33
[34]	20	200	1	30	28.31	55.95	0.33
[34]	50	200	1	30	28.31	55.95	0.33
[34]	100	200	1	30	28.31	55.95	0.33
[34]	30	120	0.604	30	28.31	55.95	0.33
[35]	100	200	0.6185	1	16.66	25.429	0.21
[35]	400	200	0.6098	1	16.66	25.429	0.21
[35]	400	200	0.2525	1	16.66	25.429	0.21
[35]	400	300	0.5308	1	16.66	25.429	0.21
[10,16]	50	50	0.731	6	12	44	8.33
[10,16]	100	50	1	6	13	40	11.82
[10,16]	50	100	0.497	6	12	44	8.33
[10,16]	100	100	0.694	6	13	40	11.82
[10,16]	50	200	0.239	6	12	44	8.33
[10,16]	100	200	0.337	6	13	40	11.82
[10,16]	50	400	0.091	6	12	44	8.33
[10,16]	100	400	0.155	6	13	40	11.82

Table 2
Soil properties of data base for testing ANN.

Reference	Net confining pressure (kPa)	Suction (kPa)	χ	h_b (kPa)	θ_r	θ_s	λ
[33]: CW	50	120	0.9069	27	8.76	52	0.94
[33]: CW	50	155	0.8053	27	8.76	52	0.94
[33]: CW	50	256	0.5376	27	8.76	52	0.94
[33]: CW	100	82	0.9953	27	8.76	52	0.94
[33]: CW	100	120	0.9335	27	8.76	52	0.94
[33]: CW	100	155	0.7744	27	8.76	52	0.94
[33]: CW	100	242	0.5621	27	8.76	52	0.94
[33]: CW	150	123	0.7937	27	8.76	52	0.94
[33]: CW	150	155	0.7434	27	8.76	52	0.94
[33]: CW	150	250	0.5313	27	8.76	52	0.94
[33]: CW	200	80	1	27	8.76	52	0.94
[33]: CW	200	151	0.7737	27	8.76	52	0.94
[33]: CW	200	242	0.5687	27	8.76	52	0.94
[33]: CW	250	80	0.8802	27	8.76	52	0.94
[33]: CW	250	120	0.8268	27	8.76	52	0.94
[33]: CW	250	148	0.811	27	8.76	52	0.94
[33]: CW	250	245	0.5748	27	8.76	52	0.94
[33]: CW	300	76	0.9265	27	8.76	52	0.94
[33]: CW	300	120	0.8002	27	8.76	52	0.94
[33]: CW	300	148	0.8218	27	8.76	52	0.94
[33]: CW	300	238	0.5715	27	8.76	52	0.94

in turn, which developed five other ANN models. Table 4 represents input neurons, architecture, activation functions and performance of these six models. The models' root mean square error values reflect their overall error performances. Model 1 has a significantly superior performance. Therefore, the effective stress parameter of unsaturated soils strongly depends on the whole soil water characteristic curve defined by the four parameters, θ_s, θ_r, $(u_a - u_w)_b$ and λ. The net mean stress also strongly influences the accuracy of the results. Table 5 presents the connection weights of model 1.

To perform a physically meaningful sensitivity analysis of the effective stress parameter, SWCC parameters of database soils were compared. A comparison of soil water characteristic curves of the Mangla Shale [30] and Hume Dam soil [31] demonstrates that, while the bubbling pressures of the soils differ significantly, other SWCC parameters are similar. We studied the sensitivity of χ to changes in bubbling pressure. Fig. 7 shows variations in χ related to the bubbling pressure obtained from the proposed ANN for different net confining stresses. This figure clearly shows that the χ parameter increases with the air entry value until it reaches a plateau close to 1. The predicted values of χ for saturated soils ($(u_a - u_w) < (u_a - u_w)_b$) were usually between 0.9 and 1.0. In other words, the proposed network underestimates the χ values of saturated soils with an error of less than 10%. This reconfirms the acceptable performance of the network.

Fig. 8 demonstrates the variation in effective stress parameters with net confining pressures while SWCC parameters remain unchanged. There is thus a threshold value for the net mean stress, below which the χ parameter strongly depends on its variation. The following arguments may explain this behavior: The SWCC

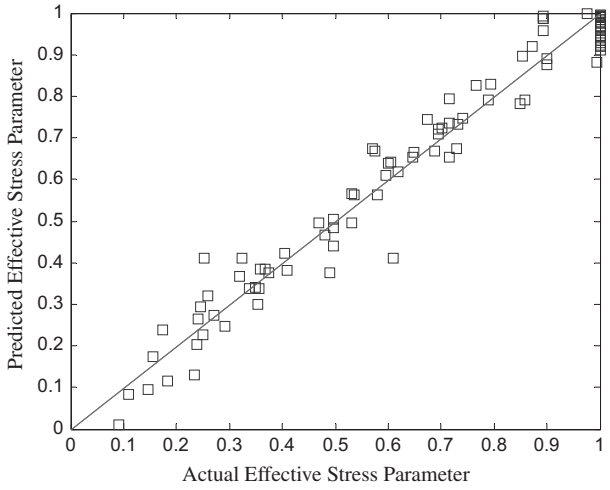

Fig. 3. Predicted versus actual χ values for training data (RMSE = 0.055, R^2 = 0.96).

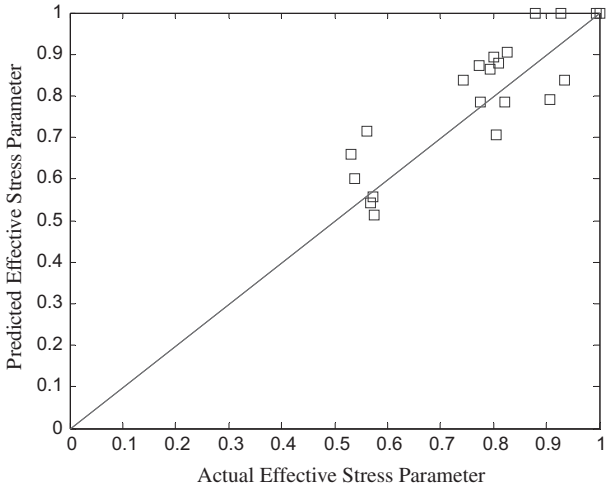

Fig. 4. Predicted versus actual χ values for testing data (RMSE = 0.083, R^2 = 0.75).

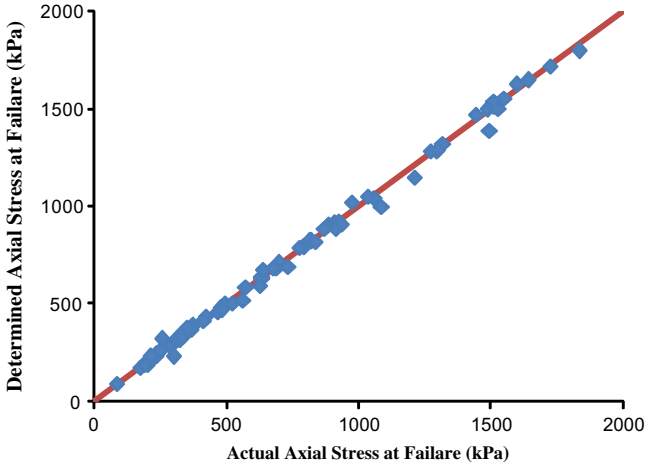

Fig. 5. Predicted versus actual values of axial stresses at failure for the training data (RMSE = 0.048, R^2 = 0.99).

parameters change with the plastic volumetric strain, and as the applied mean stress surpasses the pre-consolidation pressure, significant plastic deformation occurs. Variations in the net stress

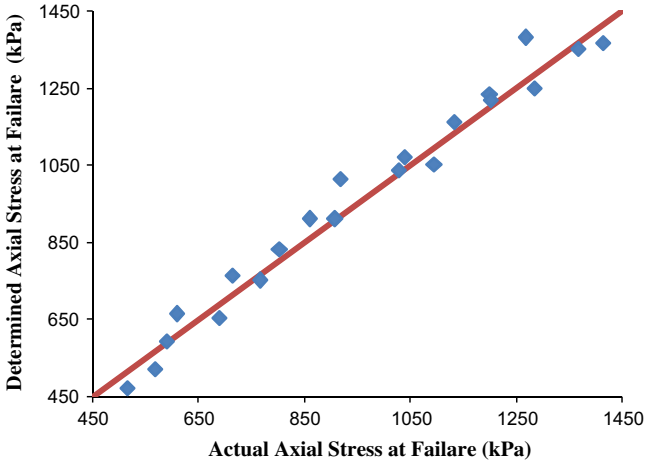

Fig. 6. Predicted versus actual values of axial stresses at failure for the testing data (RMSE = 0.053, R^2 = 0.97).

Table 3
Effective shear strength parameters of the studied soils.

Reference	Internal friction angle (°)	Effective cohesion (kPa)
Rahardjo et al. [29]	31.5	0.0
Lee et al. [7]	41.4	19.3
Khalili et al. [31]	29	5
Khalili et al. [31]	29	19
Khalili et al. [31]	30	5
Rassam and Williams [32]	41.4	0.0
Rassam and Williams [32]	40.8	0.0
Thu et al. [33]	32	0.0
Miao et al. [34]	21.3	32
Rampino et al. [35]	27.8	20
Russell and Khalil [16,10]	21.9	0.0

Table 4
Performance of ANN models.

Model	Inputs	Architecture	Activation function	RMSE (training)	RMSE (testing)
1	$\sigma_{3,net}$, suction, h_b, θ_r, θ_s, λ	6-6-1	logsig–logsig	0.055	0.083
2	$\sigma_{3,net}$, suction, θ_r, θ_s, λ	5-5-1	logsig–logsig	0.1	0.12
3	$\sigma_{3,net}$, suction, h_b, θ_s, λ	5-4-1	tansig–logsig	0.12	0.19
4	$\sigma_{3,net}$, suction, h_b, θ_r, λ	5-4-1	tansig–logsig	0.096	0.23
5	$\sigma_{3,net}$, suction, h_b, θ_r, θ_s	5-4-1	logsig–logsig	0.1	0.17
6	Suction, h_b, θ_r, θ_s, λ	5-5-1	tansig–logsig	0.12	0.13

thus affect the χ parameter considerably. However, as the rate of plastic strains decrease with the applied net stress, the influence of the stress on the χ parameter diminishes.

Furthermore, SWCCs of 14 different silty clays from the Shiraz plain in Iran, presented by Johari, helped estimate the variation of the χ parameter of these soils with suction [36]. The values of the SWCC parameters, given in Table 6, predicted the χ parameter. Fig. 9 demonstrates the range of χ for this soil when the net con-

Table 5
Connection weights for ANN model 1.

Hidden layer	Net vertical stress (kPa)	Suction (kPa)	h_b	θ_r	θ_s	λ	Input bias	Output neuron
1	0.0075	−0.0479	0.0071	0.0457	0.0062	0.0123	5.2901	−4.4094
2	0.0531	−0.0644	−0.0026	0.0179	0.0457	−0.4991	4.9236	1.9835
3	0.1860	−0.0849	0.1073	1.8144	0.0178	0.5522	4.9102	6.7515
4	0.9298	0.2585	0.3287	−0.3298	−0.1729	−1.1049	4.5907	1.4217
5	−0.4577	0.3667	−0.1913	−0.9606	0.0869	1.5809	−6.2091	2.8266
6	0.4932	−0.1343	0.2619	2.8864	−0.5184	−1.7585	−34.3200	3.4507
Output bias	–	–	–	–	–	–	–	−5.8618

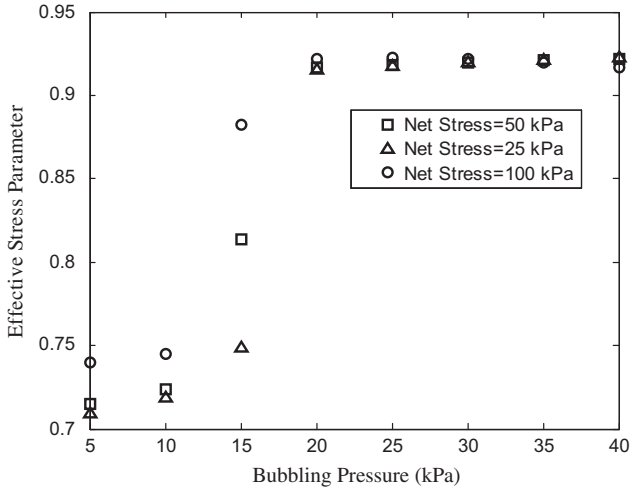

Fig. 7. Estimated variation of effective stress parameter with respect to bubbling pressure based on the Mangla Shale and Hume Dam soil properties, suction = 200 kPa, $\theta_s = 35$, $\theta_r = 20$, $\lambda = 1$.

fining pressure is 200 kPa. This figure clearly shows that the shape of the curve expressing variations of χ with suction is similar to the relationship proposed by Khalili and Khabbaz, given by Eq. (5). However, some suctions deviate from the bounds suggested by Eq. (5) in the medium range. Furthermore, the suction value corresponding to the transition from the saturated to unsaturated situation ($\chi \approx 1$) differs from the bubbling pressure determined from the pressure plate test (the modified air entry value employed in Eq. (5)). These discrepancies occur because of the dependence of the χ-parameter on the plastic volumetric strain from the applied net stress.

5. Conclusion

Both the neural network approach and the test results indicate that soil properties influence the increase in unsaturated shear strength. Performing tests on unsaturated soils is therefore a comparatively difficult, time-consuming and expensive task; the application of ANN to determine the effective stress parameter is well justified.

A feed-forward back propagation algorithm was used to determine whether an artificial neural network can predict the effective stress parameter, χ, in unsaturated soils. The ANN model could predict the target values for the training datasets. The capability of the trained ANN to predict target values for CW data that had not been encountered during training was tested and the results were promising. The results also showed good agreement between the model's prediction and the actual shear strength for both training and testing data. Additionally, network analysis indicated that the χ-parameter strongly depends on the net mean stress. This dependency is more pronounced below a threshold value that is different between soil types. Finally, the trained network estimated the variation in χ values for Shiraz silty clay for a practical range of suctions.

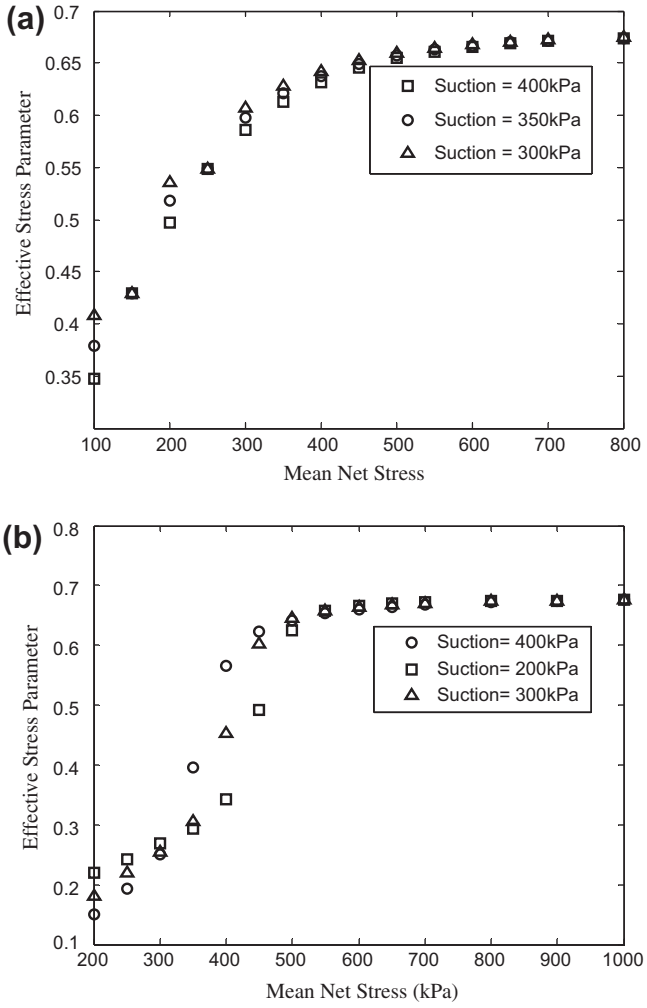

Fig. 8. Estimated variation of effective stress parameter with respect to net confining pressure: (a) bubbling pressure = 50 kPa, $\theta_s = 45$, $\theta_y = 0$, $\lambda = 0.1$. (b) Bubbling pressure = 2.5 kPa, $\theta_s = 35$, $\theta_y = 8$, $\lambda = 0.6$.

Table 6
SWCC properties for Shiraz silty clay.

References	h_b (kPa)	θ_r	θ_s	λ
Johari [36]	25	10	44	0.25

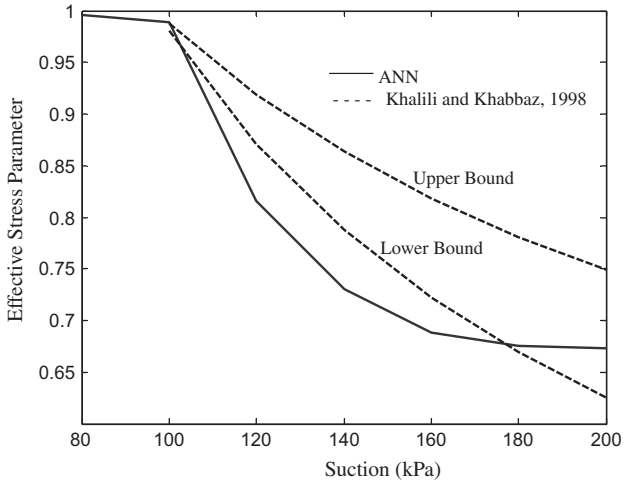

Fig. 9. Estimated range of effective stress parameter for Shiraz silty clay by ANN and Khalili and Khabbaz relationship (employing corrected bubbling pressure), net confining pressure = 200 kPa (SWCC data from Johari [36]).

The upper limit of the bubbling pressures considered in this study was 200 kPa; the validity of the ANN should therefore be used with caution for finer soils with a higher bubbling pressure.

More studies are encouraged for predicting the effective stress parameter of unsaturated soils from direct shear test results [37]. As the net mean stress affects the SWCC's shape in triaxial tests, the net vertical stress can also change the parameters of the soil water characteristic curve during the consolidation stage of direct shear tests. This requires a comprehensive database with the results of direct shear tests on unsaturated soils with the net vertical stress, instead of net mean stress.

References

[1] Bishop AW. The principle of effective stress. Teknisk Ukeblad 1959;106(39):859–63.
[2] Oberg AL, Salfors G. Determination of shear strength parameters of silts and sands based on the water retention curve. Geot Testing J, GTJODJ 1997;20(1):40–8.
[3] Loret B, Khalili N. An effective stress elasto-plastic model for unsaturated soils. Mech Mater 2002;44:97–116.
[4] Fredlund DG, Xing A, Fredlund MD, Barbour SL. The relationship of the unsaturated soil shear strength to the soil water characteristic curve. Can Geotech J 1996;33:440–8.
[5] Vanapalli SK, Fredlund DG, Pufahl DE, Clifton AW. Model for the prediction of shear strength with respect to matric suction. Can Geot J 1996;33:379–92.
[6] Garven EN, Vanapalli SK. Evaluation of empirical procedures for predicting the shear strength of unsaturated soils. In: Proceedings of the Unsaturated Soils 2006, ASCE, Sharma and Singhal; 2006. p. 2570–81.
[7] Lee IM, Sung SG, Cho GC. Effect of stress state on the unsaturated shear strength of a weathered granite. Can Geotech J 2005;42:624–31.
[8] Khalili N, Khabbaz MH. A unique relationship for the determination of the shear strength of unsaturated soils. Geotechnique 1998;48:1–7.
[9] Xu YF. Fractal approach to unsaturated shear strength. J Geotech Geoenv Eng, ASCE 2004;3:264–73.
[10] Russell AR, Khalili N. A unified bounding surface plasticity for unsaturated soils. Int J Numer Anal Methods Geomech 2006;30:181–212.
[11] Zargarbashi S, Khalili N. Discussion of "Shear strength equations for unsaturated soils under drying and wetting" by G.S. Guan, H. Rahardjo and L.E. Choon April 2010, Vol. 136, No. 4, pp. 549–606. ASCE, J Geotech Geoenv Eng, in press.
[12] Fazeli A, Habibagahi G, Ghahramani A. Shear strength characteristics of Shiraz unsaturated silty clay. Iranian J Sci Technol 2010;33(B4):327–41.
[13] Arvin MR, Karami MV, Ajdari M, Habibagahi G. A percolation approach to determination of effective stress parameter in unsaturated soils. In: Proceedings of the 3rd Asia Pacific conf on unsat soil mech, China; 2007.
[14] Lee SJ, Lee SR, Kim YS. An approach to estimate unsaturated shear strength using artificial neural network and hyperbolic formulation. Comput Geotech 2003;30:489–503.
[15] Kayadelen C. Estimation of effective stress parameter of unsaturated soils by using artificial neural network. Int J Numer Anal Methods Geomech 2008;32:1087–106.
[16] Russell AR, Khalili N. A bounding surface plasticity model for sands exhibiting particle crushing. Can Geotech J 2004;41:1179–92.
[17] Ajdari1 M, Nowamooz H, Masrouri F, Habibagahi G, Ghahramani A. Hydro-mechanical response of an expansive silt–bentonite mixture, UNSAT2010. Barcelona: Alonso and Gens; 2010. p. 175–80.
[18] White NF, Duke HR, Sanada DK, Corey AT. Physics of desaturation in porous materials. J Irrigation Drain Div, ASCE 1970;96:165–91.
[19] Bagherieh A, Khalili N, Habibagahi G, Ghahramani A. Drying response and effective stress in a double porosity aggregated soils. J Eng Geol 2009;25(1):44–50.
[20] Ajdari1 M, Habibagahi G, Nowamooz H, Masrouri F, Ghahramani A. Shear strength behavior and soil water retention curve of a dual porosity silt–bentonite mixture. Sci Iran 2010:430–40.
[21] Brooks RH, Corey AT. Hydraulic properties of porous medium. Hydrology paper, No. 3. Civ. Eng. Dep., Colorado State Univ., Fort Colins, Colo; 1964.
[22] van Genuchten MT. A closed form equation for predicting hydraulic conductivity of unsaturated soils. Soil Sci Soc Am J 1980;44(5):892–8.
[23] Fredlund DG, Xing A. Equations for the soil–water characteristic curve. Can Geotech J 1994;31:521–32.
[24] Habibagahi G, Bamdad A. A neural network framework for mechanical behavior of unsaturated soils. Can Geotech J 2003;40:684–93.
[25] Nguyen D, Widrow B. The truck backer-upper: an example of self learning in neural networks. In: International conference on neural networks, Washington, DC, 18–22 June, IEEE 2; 1989. p. 363–75.
[26] Levenberg K. A method for the solution of certain problems in least squares. Quart Appl Math 1944;2:164–8.
[27] Marquardt D. An algorithm for least squares estimation of nonlinear parameters. SIAM J Appl Math 1963;11:431–41.
[28] MATLAB. The math-works, Inc., Natick, Massachusetts; 2004.
[29] Rahardjo H, Heng OB, Choon LE. Shear strength of a compacted residual soil from consolidated drained and constant water content triaxial tests. Can Geotech J 2004;41:421–36.
[30] Bishop AW, Blight GE. Some aspects of effective stress in saturated and partially saturated soils. Geotechnique 1963;13:177–97.
[31] Khalili N, Geiser F, Blight GE. Effective stress in unsaturated soils: review with new evidences. Int J Geomech 2004;4(2):115–26.
[32] Rassam DW, Williams DJ. A relationship describing the shear strength of unsaturated soils. Can Geotech J 1999;36:363–8.
[33] Thu TM, Rahardjo H, Leong EC. Effect of hysteresis on the shear strength envelopes from constant water content and consolidated drained triaxial tests. In: Proc unasaturated soils 2006, ASCE, Sharma and Singhal; 2006. p. 1212–22.
[34] Miao L, Liu S, Lai Y. Research of soil water characteristics and shear strength of Naniang expansive soil. Eng Geol 2002;65:261–7.
[35] Rampino C, Mancuso C, Vianale F. Experimental behavior and modeling of an unsaturated compacted soil. Can Geotech J 2000;37:748–63.
[36] Johari A. Predicting soil water characteristic curve using artificial intelligence. PhD. Thesis, Shiraz University, Shiraz, Iran; 2006.
[37] Ajdari M, Habibagahi G, Ghahramani A. Predicting effective stress parameter of unsaturated soils in plane strain condition using neural networks. In: Proceedings of the 17th ICSMGE, Egypt; 2009. p. 797–800.